WPMAT-PR(18) 20617

S Dudarev et al.

# Multi-scale model for stresses, strains and swelling of reactor components under irradiation

Preprint of Paper to be submitted for publication in
Nuclear Fusion

This work has been carried out within the framework of the EUROfusion Consortium and has received funding from the Euratom research and training programme 2014-2018 under grant agreement No 633053. The views and opinions expressed herein do not necessarily reflect those of the European Commission.

# Multi-scale model for stresses, strains and swelling of reactor components under irradiation.

Sergei L. Dudarev
*UK Atomic Energy Authority, Culham Science Centre, Oxfordshire OX14 3DB, UK and Department of Materials, University of Oxford, Parks Road, Oxford OX1 3PH, UK*

Daniel R. Mason
*UK Atomic Energy Authority, Culham Science Centre, Oxfordshire OX14 3DB, UK*

Edmund Tarleton
*Department of Materials, University of Oxford, Parks Road, Oxford OX1 3PH, UK*

Pui-Wai Ma
*UK Atomic Energy Authority, Culham Science Centre, Oxfordshire OX14 3DB, UK and Department of Engineering Science, University of Oxford, Parks Road, Oxford, OX1 3PJ, UK*

Andrea E. Sand
*Department of Physics, University of Helsinki - P.O. Box 43, FI-00014 Finland*

Predicting strains, stresses and swelling in power plant components exposed to irradiation directly from the observed or computed defect and dislocation microstructure is a fundamental problem of fusion power plant design that has so far eluded a practical solution. We develop a model, free from parameters not accessible to direct evaluation or observation, that is able to provide estimates for irradiation-induced stresses and strains on a macroscopic scale, using information about the distribution of radiation defects in the microstructure. The model exploits the fact that elasticity equations involve no characteristic spatial scale, and hence admit a mathematical treatment that is an extension to that developed for the evaluation of elastic fields of defects on the nanoscale. In the analysis given below we use, as input, the radiation defect structure data derived from *ab initio* density functional calculations and large-scale molecular dynamics simulations of high-energy collision cascades. We show that strains, stresses and swelling can be evaluated using either integral equations, where the source functions are defined by the density of relaxation volumes of defects, or they can be computed from heterogeneous partial differential equations for the components of the stress tensor, where the density of body forces is proportional to the gradient of the density of relaxation volumes. We perform a case study where strains and stresses are evaluated analytically and exactly, and develop a general finite-element implementation of the method, applicable to a broad range of predictive simulations of strains and stresses induced by irradiation in materials and components of any geometry in a nuclear power plant.

## I. INTRODUCTION

One of the challenges associated with the design, construction and operation of a fusion or an advanced fission power plant is the need to predict stresses, strains, and swelling resulting from the exposure of structural components of a reactor to irradiation during operation. These stresses and strains have microscopic origin and stem from the fact that radiation defects have substantial elastic relaxation volumes[1,2], which give rise to strong local deformation of the lattice. For example, the elastic relaxation volume of a self-interstitial atom defect in tungsten, predicted by density functional theory, is $\Omega_{rel} = 1.67\Omega_0$, where $\Omega_0$ is the volume of an atom, whereas the relaxation volume of a vacancy is $\Omega_{rel} = -0.37\Omega_0$ , see e.g. Refs.[2,3]. The large positive mismatch between elastic relaxation volumes of self-interstitial and vacancy type defects in metals, which accumulate in the microstructure as a result of irradiation, gives rise to the local volumetric expansion, and produces stresses in materials exposed to irradiation, resulting in macroscopic swelling and heterogeneous deformation of reactor components.

Models for swelling developed since the 1970s focus on one particular aspect of the phenomenon, the diffusion-mediated preferential absorption of self-interstitial atom defects by dislocations[1,4–6]. There is extensive literature on the dynamics of accumulation of defects in microstructure and particularly on the evaluation of dislocation bias factors[1,7–12], which are then used as input parameters for mean-field rate theory models describing the dynamics of growth of voids in materials exposed to irradiation[4–6,13]. These mean-field models do not require, and do not evaluate, the macroscopic stresses and strains resulting from the accumulation of defects. Neither do they take into account the fact that elastic relaxation of complex defect configurations involves the accumulation of very strong local deformation of the lattice near the defects, resulting in that the relaxation volume of a complex defect cluster does not equal the sum of relaxation volumes of constituting defects. The defect configurations formed in colli-

sion cascades initiated by high-energy neutrons[14–19] have a fairly complex structure, and their relaxation volumes, locals strains and stresses are sensitive to the relative proximity of individual defects.

A particularly significant practical aspect of the problem of accumulation of radiation defects in structural materials exposed to high-energy neutron irradiation during power plant operation, which has so far eluded a satisfactory solution, is related to the fact that in a treatment of deformation of a component exposed to irradiation, not only the presence of defects in the bulk of the material, but also boundary conditions at surfaces, define the final configuration of stresses and strains. For example, it is known that the magnitude of the total elastic relaxation volume of a point defect depends on boundary conditions at surfaces of the material where it resides and, surprisingly, the role of boundary conditions does not diminish in the macroscopic limit[20,21].

Below we develop a real-space multi-scale model for strains and stresses produced in reactor components by spatially distributed complex configurations of radiation defects produced by irradiation. We show that if the properties of materials are reasonably isotropic, it is the defect relaxation volume density, i.e. the real-space distribution of relaxation volumes of self-interstitial and vacancy defects and clusters of such defects in a reactor component, that fully defines the resulting macroscopic strains and stresses. Individual defects and clusters of defects act as sources of strains and stresses, which are determined self-consistently, taking into account the appropriate boundary conditions. The fundamental notion relating macroscopic strains and stresses to microstructure are the dipole tensor and relaxation volume of a defect object, which can be an individual point defect or a large cluster of such defects formed in a collision cascade. We show that the notion of the dipole tensor of a defect, which has so far been only applied to nano-scale point defects[2,20,22], can in fact be used for characterizing defect objects of arbitrary size. This is a mere consequence of that there is no characteristic spatial scale in elasticity equations. At a large distance from an arbitrarily complex configuration of defects, for example, a cluster of defects containing thousands of individual point defects, the elastic strain generated by the cluster equals

$$\epsilon_{ij}(\mathbf{r}) = -P_{kl}\frac{\partial^2}{\partial x_j \partial x_l} G_{ik}(\mathbf{r}-\mathbf{R}), \qquad (1)$$

where $\mathbf{R}$ is the position of the defect cluster, $G_{ik}(\mathbf{r}-\mathbf{R})$ is Green's function of elasticity equations[23], and $P_{kl}$ is the dipole tensor of the defect configuration. Equation (1) fully defines the strain field generated by a defect cluster at distances that are much greater than its characteristic spatial extent.

It is well established how to compute elastic dipole tensors of point defects[2,22,24]. Below, we show how elastic dipole tensors can be defined and evaluated for defect clusters produced by the collapse of entire high-energy collision cascades. The condition that makes it possible to apply the dipole tensor concept to the treatment of strains and stresses in a reactor component is that the spatial scale of a defect object in the radiation-induced microstructure is always small in comparison with the spatial scale of a component.

Historically, elastic dipole tensors were introduced in order to treat long-range elastic fields of nano-scale point defects, and elastic interactions between such defects, as well as between defects and dislocations[20,25,26]. Still, the fact that the universal scale-free nature of elasticity equations enables extending the notion of elastic dipole tensor of a defect to mesoscopic and macroscopic scales, did not appear to have been recognized.

In the treatment of a spatially-localized defect configuration, which may include defects produced by the collapse of an entire cascade or even a group of cascades, it is only necessary to take into account the discreteness of atomic lattice in the most strongly distorted core regions of defect structures. At large distances from a defect configuration, lattice discreteness is no longer significant and the rate of variation of atomic displacements as a function of spatial coordinates is small $|\partial u_i/\partial x_j| \ll 1$. In this limit, the strain and stress fields generated by a defect configuration are fully characterized by a symmetric $3\times 3$ tensor $P_{kl}$. The volume dipole tensor density varies from one point in the material to another, depending on the local degree of exposure of a material to irradiation. The dipole tensor can be defined irrespectively of the nature of a defect object, for example, it can be defined for a point defect, a dislocation loop[2,22,26], or a fairly complex configuration of atomic displacements produced by a collision cascade as a whole. In the latter case, although the volume of the spatial region involved in the calculation of $P_{kl}$ contains a large number of atoms, it is still small in comparison with the size of a reactor component, justifying the fundamental approximation on which equation (1) is based.

In the next section we outline the formalism involved in the evaluation of stress and strain fields associated with spatially distributed defect structures. We derive the fundamental equations defining strains, stresses and displacements in an arbitrary volume of a material containing spatially distributed defects. If the material is elastically isotropic and defects have no preferred orientation, the strains and stresses are fully determined by the distribution of spatially-varying density of elastic relaxation volumes, a dimensionless function that acts as a source term in equations for the irradiation-induced stresses and strains. Then we show how the relaxation volumes of individual point defects can be computed using *ab initio* density functional theory methods, and provide accurate values of relaxation volumes computed for several metals with cubic crystal structure. Subsequently, we compare accuracy of *ab initio* and atomic relaxation methods using semi-empirical interatomic potentials, and show how to obtain accurate values of dipole tensors for entire configurations of defects produced by the collapse of collision cascades initiated by high-energy

neutrons. For both cases, we discuss a practical way of defining the density of relaxation volumes of defects and relate it to a measure of exposure of a material to neutron irradiation. We then give a full and exact solution of elasticity equations describing a spherical shell with a source of irradiation at its centre, which produces a certain spatially varying density of defects in the walls of the shell. The solution makes it possible to determine swelling, strain and stresses everywhere in the shell, and it also illustrates the pivotal part played by the boundary conditions. Finally, we discuss a finite element implementation of the method and examine a possible application of our approach to the *in silico* evaluation of operational performance of a fusion power plant.

## II. GENERAL METHODOLOGY

At a large distance from a strongly deformed atomic configuration, for example a defect or a cluster of defects, the field of displacements of atoms from their equilibrium positions in the lattice is given by the equation[20]

$$u_i(\mathbf{r}) = -P_{kl}\frac{\partial}{\partial x_l}G_{ik}(\mathbf{r}-\mathbf{R}). \qquad (2)$$

In this equation, $P_{kl}$ is the elastic dipole tensor of the defect configuration that, according to (2), fully defines the elastic field that the configuration generates in the material. $G_{ik}(\mathbf{r}-\mathbf{R})$ is the elastic Green's function[23], which in the isotropic elasticity approximation has the form

$$G_{ik}(\mathbf{r}) = \frac{1}{16\pi\mu(1-\nu)r}\left[(3-4\nu)\delta_{ik}+\frac{x_i x_k}{r^2}\right]. \qquad (3)$$

Here, $\mu$ is the shear modulus of the material and $\nu$ is the Poisson ratio, see[27]. From (2) and (3) we find

$$u_i(\mathbf{r}) = \frac{1}{16\pi\mu(1-\nu)|\mathbf{r}-\mathbf{R}|^2}\times \left[2(1-2\nu)P_{il}\eta_l-\eta_i P_{kk}+3\eta_i(\eta_k P_{kl}\eta_l)\right], \qquad (4)$$

where summation over repeated indexes is assumed, and $\eta_i=(\mathbf{r}-\mathbf{R})_i/|\mathbf{r}-\mathbf{R}|$.

Equations similar to (4) have been extensively explored in connection with the treatment of elastic fields of point defects on the nano-scale[2,22,28,29]. However, as the form of equation (4) suggests, there is no specific spatial scale at which it should be applied, as elastic fields have no intrinsic spatial scale associated with them. For example, using formula (4) one can approximate the elastic field of a fairly large defect structure just as well as it can be applied to a point defect.

The magnitude and the angular anisotropy of elastic field is described by the matrix elements of tensor $P_{kl}$, which can be evaluated using atomistic simulations with periodic boundary conditions, assuming fixed shape and size of the simulation cell, using the equation[2,20,24]

$$P_{kl} = -\int_V \sigma_{kl}(\mathbf{r})d^3r = -V\overline{\sigma}_{kl}, \qquad (5)$$

where $V$ is the volume of the simulation cell containing the defect structure, and $\overline{\sigma}_{kl}$ is the volume average stress tensor. In literature[20,24], equation (5) has so far been only applied to point defects, and hence the size of the cell used in simulations was relatively small, in most cases not exceeding $10^3$ atoms. However, since the notion of the dipole tensor defined above is entirely general, equation (5) can be applied to a defect structure of arbitrary size, potentially involving millions of atoms and many individual point defects and clusters of defects.

It is convenient to represent $P_{kl}$ is the following form

$$P_{kl} = C_{klmn}\Omega_{mn}, \qquad (6)$$

where $\Omega_{mn}$ is an auxiliary 3×3 tensor, also uniquely characterizing the defect structure, and $C_{ijkl}$ is the tensor of elastic constants. The advantage that this representation offers is that it provides a simple and robust way of computing the relaxation volume of an arbitrary complex defect configuration as a whole. Indeed, the relaxation volume of a defect configuration in an body with *surfaces free of tractions* equals[20]

$$\Omega_{rel} = S_{mmkl}P_{kl} = \Omega_{kk} = Tr\Omega, \qquad (7)$$

where $S_{ijkl}$=$(C_{ijkl})^{-1}$ is the elastic compliance tensor[30]. Tensor $\Omega_{kl}$ can be expressed in terms of its eigenvectors and eigenvalues as

$$\Omega_{mn} = \sum_{s=1}^{3}\Omega^{(s)}e_m^{(s)}e_n^{(s)}, \qquad (8)$$

where eigenvectors $\mathbf{e}^{(s)}$ form a mutually orthogonal set, and eigenvalues $\Omega^{(s)}$ have the meaning of partial relaxation volumes. They satisfy the condition

$$\Omega_{rel} = \sum_{s=1}^{3}\Omega^{(s)}, \qquad (9)$$

that, if the defect configuration has been formed as a result of a collision cascade event initiated by an energetic neutron, gives the total relaxation volume of cascade debris. Swelling, often occurring under neutron irradiation, results from the accumulation of uncompensated relaxation volumes of defects and defect clusters produced in collision cascades initiated by neutrons.

In engineering applications, where the scale of effective volumes containing defects is large, and defects and defect adopt random spatial orientations, the eigenvectors of tensor $\Omega_{mn}$ may point in any spatial direction with equal probability. For example, consider the relaxation volume tensor of a crowdion defect[2] shown schematically in Figure 1

$$\Omega_{mn} = \Omega^{(1)}l_m l_n + \frac{\Omega^{(2)}}{3}\delta_{mn}. \qquad (10)$$

The direction vector $\mathbf{l}$ of the axis of the defect can adopt any of the eight ⟨111⟩ type directions. As a result, the

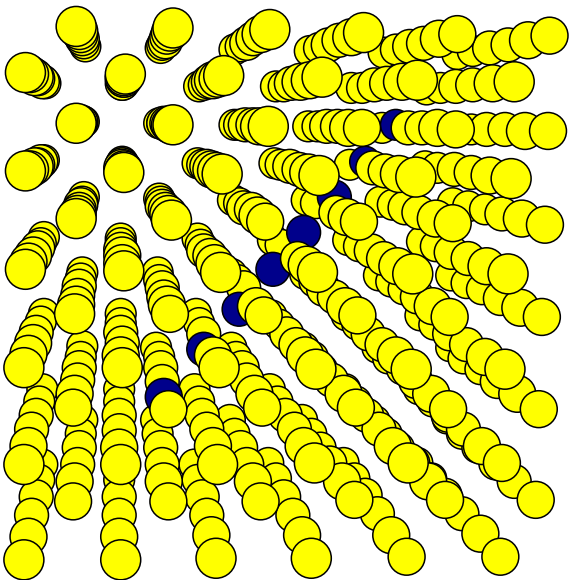

FIG. 1: A sketch of a self-interstitial crowdion defect, where the axis of the defect is parallel to the [111] crystallographic direction.

average over defect orientations relaxation volume tensor is diagonal with respect to $m$ and $n$.

Similarly, we can define an average over orientations relaxation volume tensor of a complex defect

$$\langle \Omega_{mn} \rangle = \sum_{s=1}^{3} \Omega^{(s)} \langle e_m^{(s)} e_n^{(s)} \rangle. \tag{11}$$

Here $\langle ... \rangle$ denotes averaging over all the directions in the solid angle of $4\pi$, namely

$$\langle f(\theta,\phi) \rangle = \frac{1}{4\pi} \int f(\theta,\phi) \sin\theta d\phi d\theta.$$

For a unit vector in three-dimensional space $\mathbf{e} = (\sin\theta\cos\phi, \sin\theta\sin\phi, \cos\theta)$, we find that

$$\begin{aligned} \langle e_i \rangle &= 0, \\ \langle e_i e_j \rangle &= \frac{1}{3}\delta_{ij}, \end{aligned} \tag{12}$$

and

$$\langle \Omega_{mn} \rangle = \frac{1}{3}\Omega_{rel}\delta_{mn}. \tag{13}$$

Substituting this into equation (6) we arrive at

$$\langle P_{kl} \rangle = \frac{\Omega_{rel}}{3} C_{klmm}, \tag{14}$$

which for crystals of cubic symmetry becomes

$$\langle P_{kl} \rangle = \frac{\Omega_{rel}}{3}(C_{11} + 2C_{12})\delta_{kl}. \tag{15}$$

In the isotropic elasticity limit the above equation for the dipole tensor reduces to[2,26]

$$\langle P_{kl} \rangle = \frac{2\mu}{3}\Omega_{rel}\frac{1+\nu}{1-2\nu}\delta_{kl} = B\Omega_{rel}\delta_{kl}, \tag{16}$$

where $B$ is the bulk modulus of the material.

In applications, where macroscopic elastic fields are formed as a result of superposition of microscopic fields created by millions of individual defects and defect clusters, which all adopt arbitrary orientations in the lattice, it is often sufficient to use the above isotropic approximation for the dipole tensor. The advantage offered by this approximation is that a defect object is characterized by only one parameter, its relaxation volume $\Omega_{rel}$. In some cases, for example in crystals with non-cubic symmetry or in the presence of significant external anisotropic elastic strain field, it may prove necessary to take into account the anisotropy of defect structures.

The field of elastic displacements generated by a defect object, the dipole tensor of which has the form (16), equals

$$u_i(\mathbf{r}) = \frac{\Omega_{rel}}{12\pi}\left(\frac{1+\nu}{1-\nu}\right)\frac{(\mathbf{r}-\mathbf{R})_i}{|\mathbf{r}-\mathbf{R}|^3}. \tag{17}$$

The strain field, corresponding to this field of displacements, is

$$\epsilon_{ij}(\mathbf{r}) = \frac{\Omega_{rel}}{4\pi|\mathbf{r}-\mathbf{R}|^3}\frac{1+\nu}{1-\nu}\left(\frac{1}{3}\delta_{ij} - \eta_i\eta_j\right), \tag{18}$$

where $\eta_i = (\mathbf{r}-\mathbf{R})_i/|\mathbf{r}-\mathbf{R}|$.

To compute the elastic stress associated with the strain field given by (18), we need to multiply the strain tensor by the four-index tensor of elastic constants, which in the isotropic elasticity approximation equals[21]

$$C_{ijkl} = \mu\frac{2\nu}{1-2\nu}\delta_{ij}\delta_{kl} + \mu\left(\delta_{ik}\delta_{jl} + \delta_{il}\delta_{jk}\right). \tag{19}$$

The resulting expression for the stress field generated by a defect object at $\mathbf{R}$ is

$$\sigma_{ij}(\mathbf{r}) = \frac{\mu\Omega_{rel}}{2\pi|\mathbf{r}-\mathbf{R}|^3}\frac{1+\nu}{1-\nu}\left(\frac{1}{3}\delta_{ij} - \eta_i\eta_j\right). \tag{20}$$

We now define the central notion of our treatment, the density of relaxation volumes of defects, which is a dimensionless quantity equal to the total relaxation volume of all the defect configurations in a unit volume of material

$$\omega_{rel}(\mathbf{r}) = \sum_{\alpha} \Omega_{rel}^{(\alpha)} \delta(\mathbf{r} - \mathbf{R}_\alpha), \tag{21}$$

where summation is performed over all the defect clusters $\alpha$ in the material. Because of the properties of the Dirac delta-function, if we integrate $\omega_{rel}(\mathbf{r})$ over a certain volume element in the material, only the defect clusters contained in that volume element are going to contribute

to the integral. There is a fundamental relation between the notion of the number of displacements per atom[31], which is a measure of exposure of a material to irradiation, and the density of relaxation volumes of defects that such exposure produces. Below, we show that function $\omega_{rel}(\mathbf{r})$ provides a measure of strength of sources of stresses and strains produced in materials by radiation defects.

The elastic strain, generated by all the defects produced by irradiation and distributed with certain density in the bulk of a reactor component, can be computed by integrating the point source function (18) with the density of relaxation volumes of defects (21) as

$$\epsilon_{ij}(\mathbf{r}) = \frac{1}{4\pi}\frac{1+\nu}{1-\nu}\int \frac{\omega_{rel}(\mathbf{R})}{|\mathbf{r}-\mathbf{R}|^3}\left(\frac{1}{3}\delta_{ij}-\eta_i\eta_j\right)d^3R. \quad (22)$$

We note that equation (18) follows from (22) if we assume $\omega_{rel}(\mathbf{R}) = \Omega_{rel}\delta(\mathbf{R}-\mathbf{R}_0)$.

Computing the stress generated in a material by a continuous distribution of defects involves an element of mathematical subtlety. First, we re-write equation (22) in the form

$$\epsilon_{ij}(\mathbf{r}) = -\frac{1}{12\pi}\frac{1+\nu}{1-\nu}\int \omega_{rel}(\mathbf{R})\frac{\partial^2}{\partial x_i\partial x_j}\frac{1}{|\mathbf{r}-\mathbf{R}|}d^3R. \quad (23)$$

To find the elements of the stress tensor

$$\sigma_{ij}(\mathbf{r}) = C_{ijkl}\epsilon_{ij}(\mathbf{r}), \quad (24)$$

we multiply (23) by the four-index tensor of elastic constants (19). This gives

$$\begin{aligned}\sigma_{ij}(\mathbf{r}) &= -\frac{\mu}{12\pi}\left(\frac{1+\nu}{1-\nu}\right)\left(\frac{2\nu}{1-2\nu}\right)\delta_{ij} \\ &\times\int \omega_{rel}(\mathbf{R})\frac{\partial^2}{\partial x_k^2}\frac{1}{|\mathbf{r}-\mathbf{R}|}d^3R \\ &-\frac{\mu}{6\pi}\frac{1+\nu}{1-\nu}\int \omega_{rel}(\mathbf{R})\frac{\partial^2}{\partial x_i\partial x_j}\frac{1}{|\mathbf{r}-\mathbf{R}|}d^3R, \end{aligned} \quad (25)$$

where the first term, proportional to $\delta_{ij}$, arises from the first term in (19). Noting that

$$\frac{\partial^2}{\partial x_k^2}\frac{1}{|\mathbf{r}-\mathbf{R}|} = \Delta\frac{1}{|\mathbf{r}-\mathbf{R}|} = -4\pi\delta(\mathbf{r}-\mathbf{R}),$$

we find the stress produced by a continuous distribution of defects

$$\begin{aligned}\sigma_{ij}(\mathbf{r}) &= \frac{\mu}{3}\left(\frac{1+\nu}{1-\nu}\right)\left(\frac{2\nu}{1-2\nu}\right)\delta_{ij}\omega_{rel}(\mathbf{r}) \\ &-\frac{\mu}{6\pi}\frac{1+\nu}{1-\nu}\int \omega_{rel}(\mathbf{R})\frac{\partial^2}{\partial x_i\partial x_j}\frac{1}{|\mathbf{r}-\mathbf{R}|}d^3R. \end{aligned} \quad (26)$$

The density of body forces arising from a continuous distribution of defects can now be found by differentiating the stress tensor with respect to $x_j$, namely[32]

$$\begin{aligned}f_i(\mathbf{r}) &= -\frac{\partial\sigma_{ij}(\mathbf{r})}{\partial x_j} = -\frac{2\mu}{3}\left(\frac{1+\nu}{1-\nu}\right)\frac{\partial}{\partial x_i}\omega_{rel}(\mathbf{r}) \\ &- \frac{\mu}{3}\left(\frac{1+\nu}{1-\nu}\right)\left(\frac{2\nu}{1-2\nu}\right)\frac{\partial}{\partial x_i}\omega_{rel}(\mathbf{r}). \end{aligned} \quad (27)$$

Deriving the first term in the above equation involved integration by parts

$$\begin{aligned}&-\frac{\mu}{6\pi}\frac{1+\nu}{1-\nu}\int \omega_{rel}(\mathbf{R})\frac{\partial}{\partial x_i}\frac{\partial^2}{\partial x_j^2}\frac{1}{|\mathbf{r}-\mathbf{R}|}d^3R \\ &= \frac{\mu}{6\pi}\frac{1+\nu}{1-\nu}\int \omega_{rel}(\mathbf{R})\frac{\partial}{\partial x_i}[4\pi\delta(\mathbf{r}-\mathbf{R})]d^3R \\ &= -\frac{\mu}{6\pi}\frac{1+\nu}{1-\nu}\int \omega_{rel}(\mathbf{R})\frac{\partial}{\partial X_i}[4\pi\delta(\mathbf{r}-\mathbf{R})]d^3R \\ &= \frac{2\mu}{3}\frac{1+\nu}{1-\nu}\frac{\partial}{\partial x_i}\omega_{rel}(\mathbf{r}), \end{aligned} \quad (28)$$

The addition of the two terms in (27) gives the density of body forces resulting from the accumulation of defects in the material

$$f_i(\mathbf{r}) = -\frac{2\mu}{3}\left(\frac{1+\nu}{1-2\nu}\right)\frac{\partial}{\partial x_i}\omega_{rel}(\mathbf{r}). \quad (29)$$

For completeness, we also note the expression for the field of elastic displacements produced by the defects distributed in the bulk of a reactor component with relaxation volume density (21), namely

$$\begin{aligned}u_i(\mathbf{r}) &= -\frac{1}{12\pi}\left(\frac{1+\nu}{1-\nu}\right)\frac{\partial}{\partial x_i}\int\frac{\omega_{rel}(\mathbf{R})}{|\mathbf{r}-\mathbf{R}|}d^3R \\ &= \frac{1}{12\pi}\frac{1+\nu}{1-\nu}\int \omega_{rel}(\mathbf{R})\frac{(\mathbf{r}-\mathbf{R})_i}{|\mathbf{r}-\mathbf{R}|^3}d^3R. \end{aligned} \quad (30)$$

Equations (22)-(25) fully define the elastic field generated directly by the sources of stresses and strains associated with relaxation volumes of spatially distributed radiation defects. However, these equations do not take into account the boundary conditions at surfaces, which give a surprisingly large contribution to the observed strains, stresses, and swelling. It is known that in the treatment of elastic fields of point defects, strains and stresses associated with boundary conditions have the same magnitude as strains and stresses (22)-(25) generated by the defects themselves, see for example[20,21]. Below we show that, for example, in tungsten only 59% of the observed swelling comes directly from the sources in equations relaxation volumes of defects. The remaining 41% of the effect comes from strains and stresses associated with boundary conditions.

In the next section we describe how function $\omega_{rel}(\mathbf{r})$ can be computed or estimated using *ab initio* methods and molecular dynamics simulations, and generic assumptions about the spatial distribution of radiation damage. We then investigate the case of a spherical shell containing an isotropic neutron source, representing for

example a vacuum vessel of a fusion power plant or the casing of a fissile fuel element, and solve the above equations for the stress and strain analytically. We then develop a finite element implementation of the approach described above, to enable computing strains and stresses in components of arbitrary shape and size exposed to irradiation.

## III. RELAXATION VOLUMES OF POINT DEFECTS IN BCC TRANSITION METALS AND GOLD

In this section we summarize results of *ab initio* density functional theory calculations of relaxation volumes of self-interstitial atoms (SIA) and vacancy defects in several bcc transition metals and in gold. The availability of such data is still relatively limited as the majority of density functional calculations of defects performed so far focused on the accurate evaluation of energies of defects[34–37], rather than on the evaluation of elastic properties of defects. The relaxation volume of a Frenkel pair can be approximated by the sum of relaxation volumes of an SIA and a vacancy. In non-magnetic bcc transition metals, the ⟨111⟩ dumbbell is the most stable SIA defect configuration[38]. We have evaluated the relaxation volumes of SIA and vacancy defects in vanadium, niobium, molybdenum, tantalum and tungsten using equation (5). DFT calculations were performed using the approach described in Ref. 2. Relaxation volumes of vacancies were computed using simulation boxes containing 3x3x3 bcc unit cells, using a 5x5x5 k-point mesh and the GGA-PBE functional.

Results of *ab initio* calculations of relaxation volumes of defects are summarised in Table I. The data given in the table show that the relaxation volume of a Frenkel pair is close to one atomic volume. Relaxation volumes of point defects in fcc gold (Au) were evaluated in Ref. 33. In gold, the most stable configuration of a SIA defect is a ⟨100⟩ dumbbell. The relaxation volume of a Frenkel pair in gold is close to 1.64 atomic volume, larger than in bcc transition metals.

| | $\Omega_{rel}^{SIA}$ | $\Omega_{rel}^{V}$ | $\Omega_{rel}^{FP}$ |
|---|---|---|---|
| V | 1.472 | -0.493 | 0.979 |
| Nb | 1.554 | -0.405 | 1.139 |
| Mo | 1.538 | -0.353 | 1.185 |
| Ta | 1.524 | -0.410 | 1.114 |
| W | 1.712 | -0.345 | 1.367 |
| Au | 2.02 | -0.38 | 1.64 |

TABLE I: Relaxation volume of ⟨111⟩ self-interstitial atom (SIA) dumbbell defects and vacancies in non-magnetic bcc transition metals, and of a ⟨100⟩ self-interstitial dumbbell defect and a vacancy in fcc gold. The relaxation volume of a Frenkel pair is approximated by the sum of relaxation volumes of a SIA defect and a vacancy. Data are given in atomic volume units; defect relaxation volumes in gold are taken from Ref. 33.

## IV. VALIDATION OF MD DATA AGAINST DFT CALCULATIONS

To compare defect dipole tensors computed using semi-empirical many-body interatomic potentials with *ab initio* results derived from density functional calculations, we evaluated dipole tensors of point defects in tungsten.
.

All the *ab initio* calculations were performed using Vienna Ab initio Simulation Package (VASP)[39–42]. We used the PBE[43,44] and AM05[45–47] exchange-correlation functionals. Plane wave energy cutoff was 450 eV. We used a supercell containing 4x4x4 bcc unit cells, and a 5x5x5 k-points mesh. First, we created perfect lattice cells containing 128 atoms and fully relaxed them, to find the equilibrium lattice parameter. Then, we created cells containing point defects. Ionic positions were relaxed, but the cell size and shape remained the same as in the perfect lattice case. Elastic dipole tensors were computed from macro-stresses using equation (5).

We have also evaluated dipole tensors of point defect using molecular statics and semi-empirical interatomic potentials. We used the Marinica (EAM4)[48] and DND potentials[38]. Similarly to *ab initio* calculations, we first fully relaxed a simulation box containing 80x80x80 perfect bcc unit cells. Then, we inserted or removed atoms in the cell, creating point defects. This was followed by the relaxation of atomic configurations, where again we did not change the cell size and shape. The dipole tensors were computed using equation (5). Comparison of elements of dipole tensors computed using density functional theory and semi-empirical potentials show that whereas the results agree qualitatively, there are significant differences between the absolute values. This is perhaps not surprising since the main criterion used in fitting the semi-empirical potentials to *ab initio* data has been the agreement between the energies of atomic configurations. Elastic properties of defects has so far received little attention although, as we show in this study, they play a pivotal part determining the magnitude of strains and stresses in reactor components under irradiation.

The defect relaxation volume density (21) can be evaluated from the computed values of relaxation volumes of SIA and vacancy defects using the equation

$$\omega_{rel}(\mathbf{r}) = \Omega_{rel}^{(SIA)} n_{SIA}(\mathbf{r}) + \Omega_{rel}^{V} n_V(\mathbf{r}), \qquad (31)$$

where $n_{SIA}(\mathbf{r})$ and $n_V(\mathbf{r})$ are the volume densities of self-interstitial atom and vacancy defects. When using this equation one has to bear in mind that while the densities of defects are positive quantities, the relaxation volume of a SIA defect is positive whereas the relaxation volume of a vacancy is negative.

| PBE | $P_{11}$ | $P_{22}$ | $P_{33}$ | $P_{12}$ | $P_{23}$ | $P_{31}$ |
|---|---|---|---|---|---|---|
| 100dumbbell | 65.92 | 53.38 | 53.38 | 0.00 | 0.00 | 0.00 |
| 110dumbbell | 56.96 | 52.56 | 52.56 | 0.00 | 11.28 | 0.00 |
| 111crowdion | 52.74 | 52.74 | 52.74 | 13.15 | 13.15 | 13.15 |
| 111dumbbell | 52.75 | 52.75 | 52.75 | 13.13 | 13.13 | 13.13 |
| Octa | 52.74 | 52.74 | 67.21 | 0.00 | 0.00 | 0.00 |
| Tetra | 47.36 | 59.11 | 59.11 | 0.00 | 0.00 | 0.00 |
| vacancy | -9.98 | -9.98 | -9.98 | 0.00 | 0.00 | 0.00 |

TABLE II: Elastic dipole tensors of point defects in tungsten. The values were computed using density functional theory with the PBE exchange-correlation functional. All the values are in eV units.

| AM05 | $P_{11}$ | $P_{22}$ | $P_{33}$ | $P_{12}$ | $P_{23}$ | $P_{31}$ |
|---|---|---|---|---|---|---|
| 100dumbbell | 66.34 | 53.85 | 53.85 | 0.00 | 0.00 | 0.00 |
| 110dumbbell | 57.37 | 53.71 | 53.71 | 0.00 | 11.77 | 0.00 |
| 111crowdion | 53.84 | 53.84 | 53.84 | 13.24 | 13.24 | 13.24 |
| 111dumbbell | 53.84 | 53.84 | 53.84 | 13.22 | 13.22 | 13.22 |
| Octa | 53.26 | 53.26 | 68.30 | 0.00 | 0.00 | 0.00 |
| Tetra | 48.13 | 59.93 | 59.93 | 0.00 | 0.00 | 0.00 |
| vacancy | -10.95 | -10.95 | -10.95 | 0.00 | 0.00 | 0.00 |

TABLE III: Elastic dipole tensors of point defects in tungsten. The values were computed using density functional theory and the AM05 exchange-correlation functional. All the values are in eV units.

| Marinica | $P_{11}$ | $P_{22}$ | $P_{33}$ | $P_{12}$ | $P_{23}$ | $P_{31}$ |
|---|---|---|---|---|---|---|
| 100dumbbell | 49.85 | 40.12 | 40.12 | 0.00 | 0.00 | 0.00 |
| 110dumbbell | 52.91 | 53.69 | 53.69 | 0.00 | 13.24 | 0.00 |
| 111crowdion | 35.16 | 35.16 | 35.16 | 14.82 | 14.82 | 14.82 |
| 111dumbbell | 37.16 | 37.16 | 37.16 | 16.59 | 16.59 | 16.59 |
| Octa | 45.10 | 45.10 | 59.77 | 0.00 | 0.00 | 0.00 |
| Tetra | 48.02 | 49.94 | 49.94 | 0.00 | 0.00 | 0.00 |
| vacancy | -1.07 | -1.07 | -1.07 | 0.00 | 0.00 | 0.00 |

TABLE IV: Elastic dipole tensors of point defects in tungsten. The values given in this table were computed using the Marinica (EAM4) semi-empirical interatomic potential for tungsten. All the values are in eV units.

| DND | $P_{11}$ | $P_{22}$ | $P_{33}$ | $P_{12}$ | $P_{23}$ | $P_{31}$ |
|---|---|---|---|---|---|---|
| 100dumbbell | 55.70 | 23.49 | 23.49 | 0.00 | 0.00 | 0.00 |
| 110dumbbell | 32.60 | 33.97 | 33.97 | 0.00 | 3.70 | 0.00 |
| 111crowdion | 36.98 | 36.98 | 36.98 | 13.64 | 13.64 | 13.64 |
| 111dumbbell | 38.21 | 38.21 | 38.21 | 13.65 | 13.65 | 13.65 |
| Octa | 25.54 | 25.54 | 60.66 | 0.00 | 0.00 | 0.00 |
| Tetra | 18.15 | 43.65 | 43.65 | 0.00 | 0.00 | 0.00 |
| vacancy | -3.33 | -3.33 | -3.33 | 0.00 | 0.00 | 0.00 |

TABLE V: Elastic dipole tensors of point defects in tungsten. The values given in this table were computed using the Derlet-Nguyen-Manh-Dudarev (DND) semi-empirical interatomic potential for tungsten. All the values are in eV units.

## V. EVALUATION OF DIPOLE TENSORS FROM ATOMISTIC CALCULATIONS

### A. The dipole tensor for a large, complex defect

Equation (2) gives the displacement field at a position $\mathbf{r}$, which is sufficiently far away from a defect so it can be treated as a point source of elastic deformation. If there are $m$ such point sources, the displacement field at $\mathbf{r}$ is simply the sum over their contributions. Contributing point sources could be a substitutional atom whose local environment induces a stress upon it, but equally could be a point-defect, or cluster of defects, viewed from a distance. The dipole tensor of a large, complex defect therefore has the same simple physical interpretation as that of a point defect or s small defect cluster - it can be approximated by a point source of stress which produces the same displacement field (to leading order) as the sum of its contributing parts.

We can say that a complex defect is a group of $m$ contributors, where the $a = \{1, 2, \ldots, m\}^{th}$ contributor has dipole tensor $P^a_{kl}$ and position $\mathbf{R}^a$. We would like to represent this with a single dipole tensor $P_{kl}$ at position $\mathbf{R}$. The displacement at $\mathbf{r}$ due to the group of $m$ contributors is

$$\begin{aligned} u_i(\mathbf{r}) &= -\sum_{a=1}^{m} P^a_{kl} \frac{\partial}{\partial x_l} G_{ik}(\mathbf{r} - \mathbf{R^a}) \\ &= -\sum_{a=1}^{m} P^a_{kl} \frac{\partial}{\partial x_l} G_{ik}(\mathbf{r} - \mathbf{R}) \\ &\quad + \sum_{a=1}^{m} \left(R^a_j - R_j\right) P^a_{kl} \frac{\partial^2}{\partial x_l \partial x_j} G_{ik}(\mathbf{r} - \mathbf{R}) \\ &\quad + \mathcal{O}\left(\frac{(\mathbf{R}^a - \mathbf{R})^2}{R^5}\right). \end{aligned} \tag{32}$$

We recognize the first term as the displacement field due to a single defect of strength $P_{kl} = \sum_a P^a_{kl}$ at $\mathbf{R}$, and the second term as the first-order correction due to the spatial extent of the defect. The spherical average of the second derivative of $G_{ik}$ is zero, so to minimise the second term we choose

$$\begin{aligned} \mathbf{R} &= \operatorname{argmin} \left\| \sum_{a=1}^{m} (\mathbf{R^a} - \mathbf{R}) \; P^a_{kl} \right\| \\ &\simeq \frac{\sum_{a=1}^{m} \|\mathbf{P}^a\| \, \mathbf{R}^a}{\sum_{a=1}^{m} \|\mathbf{P}^a\|} \end{aligned} \tag{33}$$

where $\|\mathbf{P}\| = \sqrt{\mathrm{Tr}(\mathbf{P}^2)}$ is the Frobenius norm, used here as a measure of the strength of the $a^{th}$ contributor. In this way we can define a single dipole tensor and single position for a complex defect.

### B. Dipole tensor for defects generated by a collision cascade

In this section we compute the dipole tensors for collision cascades in bulk tungsten simulated with classical molecular dynamics. It is not our intention here to provide an exhaustive database of values of dipole tensors, only to describe the relative ease of such a calculation. For an empirical potential we can define the energy as a sum over all atoms $a$, and so[49]

$$P_{kl} \equiv \sum_a P^a_{kl} = -\frac{1}{2}\sum_{a,b} f_{ab,k} \otimes r_{ab,l}, \qquad (34)$$

where $f_{ab,k}$ is the $k$th Cartesian component of the force acting on atom $a$ due to atom $b$ and $r_{ab,l}$ is the $l$th Cartesian component vector separation between them. The second derivative of energy with respect to strain gives the (fourth-rank) elastic constant tensor, needed for evaluating the relaxation volume given by equation (7).

Collision cascades were simulated with the classical molecular dynamics code PARCAS. A simulation supercell of 6.8 million atoms at 0K was established with periodic stress-free boundary conditions, then a cascade was initiated by giving a single atom a large kinetic energy (100keV - 200keV) in a random direction. The DND interatomic potential for tungsten by Derlet et al.[38], stiffened at short range by Björkas et al.[50], was used for the simulations, and a non-local friction force was applied to atoms with a kinetic energy above 10 eV to account for energy loss due to electronic stopping[51]. A Berendsen thermostat[52] set to 0 K was applied to the atoms in a 1.5 unit cell thick region along all periodic boundaries. Cascades were followed for 40 ps, at which point further defect evolution is thermal rather than ballistic. Details of the simulation method can be found in Ref.[15]. Similar cascade simulations have been shown to reproduce the observed experimental cluster size-frequency distribution[16,53] and spatial extent[19]. A typical relaxed cascade configuration is shown in Figure 2. To compute the dipole tensor for the atomically relaxed configuration, the atoms in the supercell could in principle be directly relaxed with conjugate gradients or a similar method, but in practice we have found that the dipole tensor converges rather slowly in a large box, and a standard convergence criteria based on force-per-atom or total energy difference alone may return without a well-converged dipole tensor. Instead we take the calculation as a three-stage procedure: first the atoms deviating more than $^1/_4$ lattice parameter from crystal positions were identified, and a buffer of four unit cells in all directions was added. A smaller rectangular cell containing these atoms was cropped from the cascade and fully relaxed. At this point the dipole tensor is converged to within 10%. The smaller cell was then re-embedded into a 4 million atom perfect crystal supercell ($128 \times 128 \times 128$ unit cells), and relaxed again. The dipole tensor is computed after the second relaxation. Finally the dipole tensor computed for the perfect crystal lattice at the original supercell size was computed and subtracted - this may not be exactly zero

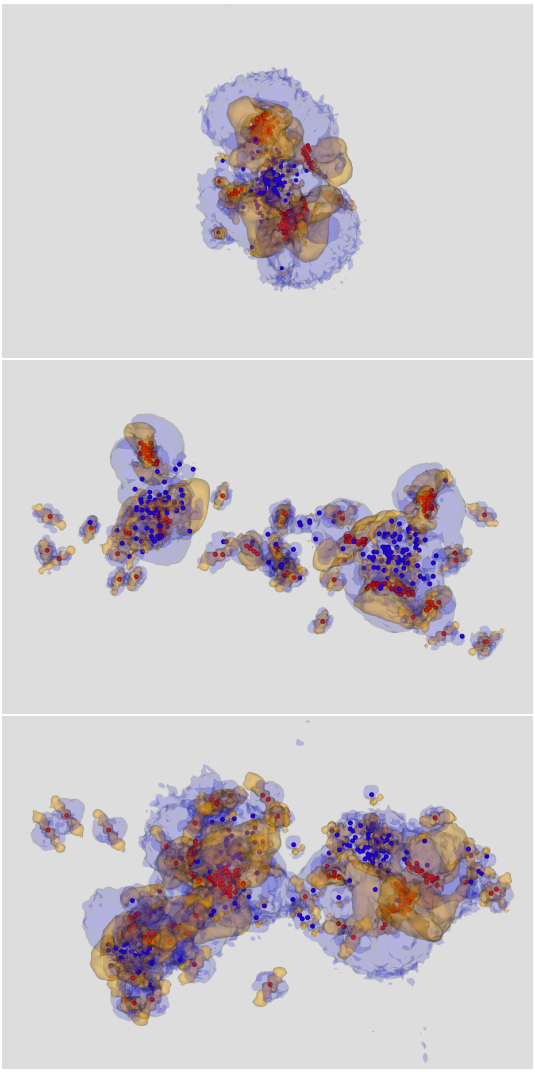

FIG. 2: Typical high-energy displacement cascades in tungsten, evolved to 40ps and then atomically relaxed at constant volume. The initial energies of recoil atoms giving rise to a cascade event: top to bottom: 100keV PKA, 150keV, 200keV. Vacancies (blue) and interstitials (red) have been identified using a Wigner-Seitz cell analysis. The defect clusters introduce both compressive and rarefactive stresses. Yellow isosurfaces show the region where atoms contribute Tr(P) = +0.15eV per atom to the dipole tensor (compressive stress), blue isosurfaces where Tr(P) = -0.05eV per atom (rarefactive) computed using equation 34. Details of these simulations are given in the text and table VI. The classic cascade structure of vacancy-rich core surrounded by interstitial clusters can be observed. From a distance, the structure of the cascade is immaterial, and the long-range elastic field of the cascade can be computed from a single dipole tensor capturing the sum of the contributions from each defect cluster formed in a cascade. Images rendered using Ovito[54].

if the lattice parameter is only specified to a fixed precision, and needs removing as it scales with system size. We find convergence in the dipole tensor to better than 1% precision after a few hours cpu time. We expect this precision to be significantly better than the accuracy of the potentials or the description of the cascade structure.

Dipole tensors were computed for isolated defects and relaxed cascade configurations using the stress method, equation (5). Results for idealised isolated defects are given in section IV, from which we conclude that empirical potentials give reasonable results. We note that the relaxation volume for a single tungsten SIA is around 1.7 $\Omega_0$, but for a large loop containing $N$ interstitials the relaxation volume drops to $N\Omega_0$, in agreement with elasticity analysis[2,26]. Defect dipole tensors for the full cascades are given in table VI. We conclude that the relaxation volume of a cascade scales with the number of Frenkel pairs, with the DND potential giving

$$\Omega_{rel} \simeq 0.5 N_{FP}\, \Omega_0 \tag{35}$$

The elastic relaxation volume density $\omega_{rel}(\mathbf{r})$ of cascades resulting from atomic recoil of energy $E$ can be computed as

$$\omega_{rel}(\mathbf{r}) = \int n(\mathbf{r}, E)\Omega_{rel}(E) dE, \tag{36}$$

where $n(\mathbf{r}, E)$ is the spatial density of cascades with energy $E$ and $\Omega_{rel}(E)$ is the relaxation volume of defects produced in a cascade initiated by a recoil atom of energy $E$. In practice, this function can be computed using neutron transport calculations for a realistic reactor geometry[55,56] followed by the evaluation of local spectra of primary knock-off atoms[57] and the treatment of the subsequent evolution of microstructure, including modelling dislocation climb[58], self-climb[59], and the formation of a network of dislocations, voids and gas bubbles.

| PKA energy (keV) | 100 | 150 | 200 |
|---|---|---|---|
| Number of Frenkel pairs | 199 | 174 | 198 |
| Elements of the dipole tensor (eV) | | | |
| $P_{11}$ | 2340 | 3080 | 3640 |
| $P_{22}$ | 1480 | 2860 | 3410 |
| $P_{33}$ | 2030 | 2450 | 3140 |
| $P_{23}$ | −907 | 62 | −1420 |
| $P_{31}$ | −1580 | −335 | 351 |
| $P_{12}$ | −367 | 1700 | −714 |
| Partial relaxation volumes $\Omega^{(s)}$ (Å$^3$) | | | |
| $\Omega_1$ | −1570 | −1150 | −908 |
| $\Omega_2$ | 505 | 331 | 2220 |
| $\Omega_3$ | 2040 | 2220 | 2240 |
| Relaxation volumes $\Omega_{rel}/\Omega_0$ | 61.4 | 88.2 | 107.0 |

TABLE VI: Results for the dipole tensor for three representative displacement cascades simulated using molecular dynamics. The energy of the initial primary knock-on atom (PKA) is given in kiloelectron-Volts (keV), the number of Frenkel Pairs was computed by the Wigner-Seitz cell analysis of the final cascade configuration. The partial relaxation volumes were computed using equation 8. The total relaxation volume of a cascade is also reported as a multiple of the volume per atom, $\Omega_0$. Elements of dipole tensors and relaxation volumes are converged to better than 1%.

## VI. STRAINS, STRESSES AND SWELLING IN A SPHERICAL SHELL: AN EXACT SOLUTION

Above, we showed how to compute the relaxation volume density (21) using *ab initio* calculations and molecular dynamics simulations of high energy collision cascades. In this and the next sections we show how to solve the elasticity equations and compute strains, stresses and swelling of components assuming that function $\omega_{rel}(\mathbf{r})$ is known. In this section, we show how to solve equations (23)-(30) analytically, and in the next section we describe a numerical finite element approach.

Consider a component, for example the vacuum vessel of a fusion power plant or the casing of a fuel cell containing fissile nuclear fuel, which we assume has the form of a spherical shell sketched in Figure 3.

If the source of neutrons inside the shell is isotropic then the distribution of defect relaxation volumes in the material depends only on the distance $r$ to the centre of the shell and is independent on the polar and azimuthal angles $\theta$ and $\phi$ of the spherical system of coordinates, the origin of which is at the centre of the shell.

The solution that we are interested in is defined on the interval $R_1 \le r \le R_2$, where $R_1$ is the inner radius of the shell and $R_2$ is its outer radius. The field of displacements is radially-symmetric and the vector of displacements can be written as $\mathbf{u}(\mathbf{r}) = u_r(r)\mathbf{n}$, where $\mathbf{n} = \mathbf{r}/r$. Differentiating equation (30), we find

$$\begin{aligned}
\frac{\partial}{\partial x_i} u_i(\mathbf{r}) &= -\frac{1}{12\pi}\left(\frac{1+\nu}{1-\nu}\right)\frac{\partial^2}{\partial x_i^2}\int \frac{\omega_{rel}(\mathbf{R})}{|\mathbf{r}-\mathbf{R}|} d^3R \\
&= \frac{1}{12\pi}\left(\frac{1+\nu}{1-\nu}\right)\int \omega_{rel}(\mathbf{R})[4\pi\delta(\mathbf{r}-\mathbf{R})] d^3R \\
&= \frac{1}{3}\left(\frac{1+\nu}{1-\nu}\right)\omega_{rel}(\mathbf{r}).
\end{aligned} \tag{37}$$

The above equation has a simple meaning, namely that it is the density of relaxation volumes of defects is what causes the material to expand or contract a result of accumulation of defects in the material. Note the remarkable prefactor $(1/3)(1+\nu)/(1-\nu)$ in the above equation, the numerical value of which is close to 0.6 for tungsten. This prefactor shows that the direct deformation of the lattice caused by the accumulation of defects is only partially responsible for the observed dimensional changes occurring as a result of irradiation. The other, similar in its magnitude, contribution comes from the boundary conditions at surfaces, as we prove below.

Since the field of displacements is radially symmetric, we apply the divergence theorem to equation (37) and

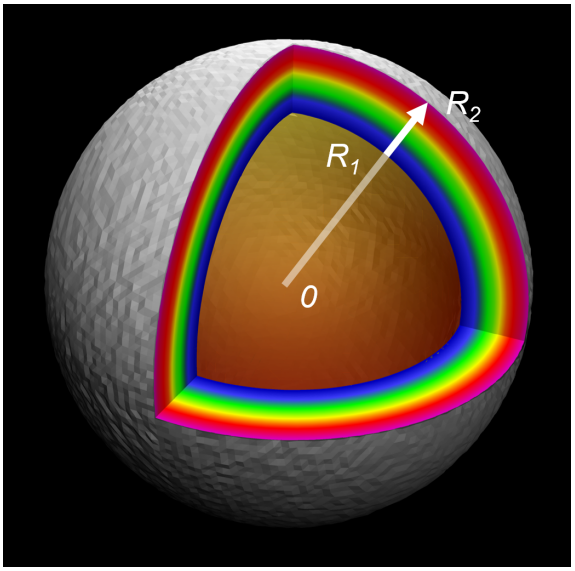


FIG. 3: A sketch of a spherical shell containing a source of neutrons in its central part. The solution described in this section gives the distribution of stresses and strains in the material of the shell for $R_1 \le r \le R_2$.

write

$$4\pi r^2 u_r(r) = \frac{4\pi}{3}\left(\frac{1+\nu}{1-\nu}\right)\int_{R_1}^{r} R^2\omega_{rel}(R)dR, \qquad (38)$$

for $R_1 \le r \le R_2$.

Noting that in the absence of radiation defects the divergence of $\mathbf{u}(\mathbf{r})$ is a harmonic function of coordinates[32], we write the field of displacements as a sum of the partial solution of heterogeneous equation (37) and a general solution of the corresponding homogeneous equation, namely

$$u_r(r) = ar + \frac{b}{r^2} + \frac{1}{3r^2}\left(\frac{1+\nu}{1-\nu}\right)\int_{R_1}^{r} R^2\omega_{rel}(R)dR. \qquad (39)$$

Here $a$ and $b$ are constants that need to be determined from boundary conditions at $r = R_1$ and $r = R_2$. Assuming that pressure at $R_1$ and $R_2$ is negligible in comparison with the stresses developing in the material due to the accumulation of defects, we adopt the traction free boundary conditions[20] $\sigma_{ij}(r)n_j = 0$ at $r = R_1$ and $r = R_2$.

Strains can be found by differentiating (39). They have the form

$$\begin{aligned}\epsilon_{ij}(r) &= a\delta_{ij} + \frac{b}{r^3}\left(\delta_{ij} - 3n_in_j\right) \\ &+ \frac{1}{3r^3}\left(\frac{1+\nu}{1-\nu}\right)\left(\delta_{ij} - 3n_in_j\right)\int_{R_1}^{r} R^2\omega_{rel}(R)dR \\ &+ \frac{1}{3}\left(\frac{1+\nu}{1-\nu}\right)n_in_j\omega_{rel}(r). \qquad (40)\end{aligned}$$

To find stresses, we need to multiply the above expression for the strain tensor by the four-index tensor of elastic constants (19). The resulting expression has the form

$$\begin{aligned}\sigma_{ij}(r) &= 2\mu a\left(\frac{1+\nu}{1-2\nu}\right)\delta_{ij} + \frac{2\mu b}{r^3}(\delta_{ij} - 3n_in_j) \\ &+ \frac{2\mu}{3r^3}\left(\frac{1+\nu}{1-\nu}\right)(\delta_{ij} - 3n_in_j)\int_{R_1}^{r} R^2\omega_{rel}(R)dR \\ &+ \frac{\mu}{3}\left(\frac{1+\nu}{1-\nu}\right)\omega_{rel}(r)\left(\frac{2\nu}{1-2\nu}\delta_{ij} + 2n_in_j\right). \qquad (41)\end{aligned}$$

Applying the traction-free boundary conditions at $r = R_1$ and $r = R_2$ to (41), we find parameters $a$ and $b$, namely

$$a = \frac{1}{6\pi}\left(\frac{1-2\nu}{1-\nu}\right)\frac{\Omega_{tot}}{R_2^3 - R_1^3}, \qquad (42)$$

and

$$b = \frac{1}{12\pi}\left(\frac{1+\nu}{1-\nu}\right)\frac{R_1^3}{R_2^3 - R_1^3}\Omega_{tot}, \qquad (43)$$

where

$$\Omega_{tot} = 4\pi\int_{R_1}^{R_2} R^2\omega_{rel}(R)dR$$

is the total relaxation volume of all the defects in the material of the shell.

The total macroscopic change of volume resulting from the accumulation of defects in the materials of the shell is given by the integral of the trace of the *full* strain tensor (40) over the volume of the component

$$\begin{aligned}\Delta V &= \int \epsilon_{ii}(\mathbf{r})dV = \int\left[\frac{1}{3}\left(\frac{1+\nu}{1-\nu}\right)\omega_{rel}(\mathbf{r}) + 3a\right]dV \\ &= \int_{R_1}^{R_2}\left[\frac{1}{3}\left(\frac{1+\nu}{1-\nu}\right)\omega_{rel}(r) + 3a\right]4\pi r^2 dr, \qquad (44)\end{aligned}$$

where we noted that $\delta_{ii} = 3$ and $n_in_i = 1$. The integration of the first term in square brackets over the volume of the shell gives

$$\Delta V_1 = \frac{1}{3}\left(\frac{1+\nu}{1-\nu}\right)\Omega_{tot},$$

whereas the second term in (44), proportional to $a$ and arising from the boundary conditions, contributes

$$\Delta V_2 = \frac{2}{3}\left(\frac{1-2\nu}{1-\nu}\right)\Omega_{tot}$$

to the total macroscopic swelling of the shell. The sum of these two terms equals $\Omega_{tot}$, confirming that swelling

is as much an effect of direct expansion of the lattice due to the accumulation of defects in the material, as it is an effect associated with boundary conditions and arising from long-range stresses and strains of defects interacting with the boundaries of the component.

Substituting (42) and (43) into (39), we find radial displacements of the inner and outer surfaces of the shell

$$\begin{aligned} u_r(R_1) &= \frac{1}{4\pi}\frac{R_1}{R_2^3-R_1^3}\Omega_{tot} \\ u_r(R_2) &= \frac{1}{4\pi}\frac{R_2}{R_2^3-R_1^3}\Omega_{tot}. \end{aligned} \quad (45)$$

These displacements satisfy the condition

$$4\pi R_2^2 u_r(R_2) - 4\pi R_1^2 u_r(R_1) = \Omega_{tot}, \quad (46)$$

which provides an alternative way of evaluating the total volumetric swelling of the shell. A remarkable property of equations (45) is that they show that both the inner and outer surfaces of an irradiated spherical shell relax outwards. The magnitude of surface displacements can be substantial. For example, the surface of a vacuum vessel with the inner radius of $R_1 = 5$ meters, after exposure to neutron irradiation, producing constant homogeneous defect relaxation volume density $\omega_{rel} = 1\%$ in the material, moves outwards by approximately $u_r(R_1) = \omega_{rel}R_1/3 \approx 1.6$ cm.

We can now find elements of the stress tensor developing in the spherical shell as a result of its exposure to irradiation. The radial diagonal element of the stress tensor is

$$\begin{aligned} \sigma_{rr}(r) &= \frac{\mu}{3\pi}\left(\frac{1+\nu}{1-\nu}\right)\left[\frac{\Omega_{tot}}{R_2^3-R_1^3}\left(1-\frac{R_1^3}{r^3}\right)\right] \\ &- \frac{\mu}{3\pi}\left(\frac{1+\nu}{1-\nu}\right)\left[\frac{4\pi}{r^3}\int_{R_1}^{r} R^2\omega_{rel}(R)dR\right] \\ &+ \frac{2\mu}{3}\left(\frac{1+\nu}{1-2\nu}\right)\omega_{rel}(r). \end{aligned} \quad (47)$$

The circumferential (hoop) components $\sigma_{\theta\theta}(r)$ and $\sigma_{\phi\phi}(r)$ of the stress tensors are

$$\begin{aligned} \sigma_{\theta\theta}(r) &= \frac{\mu}{3\pi}\left(\frac{1+\nu}{1-\nu}\right)\left[\frac{\Omega_{tot}}{R_2^3-R_1^3}\left(1+\frac{R_1^3}{2r^3}\right)\right] \\ &+ \frac{\mu}{6\pi}\left(\frac{1+\nu}{1-\nu}\right)\left[\frac{4\pi}{r^3}\int_{R_1}^{r} R^2\omega_{rel}(R)dR\right] \\ &+ \frac{\mu}{3}\left(\frac{1+\nu}{1-\nu}\right)\left(\frac{2\nu}{1-2\nu}\right)\omega_{rel}(r). \end{aligned} \quad (48)$$

Due to the spherical symmetry of the problem, we have $\sigma_{\theta\theta}(r) = \sigma_{\phi\phi}(r)$. The above formulae are valid for any distribution of defect relaxation volume density $\omega_{rel}(r)$ in the spherical shell, which is a function of radial variable $r$.

As the density of defects vanishes in the immediate vicinity of free surfaces and hence $\omega_{rel}(R_1) = \omega_{rel}(R_2) = 0$. The radial stress (47) also vanishes at surfaces at $r = R_1$ and $r = R_2$, but the hoop stress (48) remains finite everywhere on the interval $R_1 \le r \le R_2$. The high radial and hoop stresses developing as a result of accumulation of defects in the material are responsible for the loss of structural integrity of the component in the limit where the relaxation volume density of defects exceeds a certain critical level.

Applications of the above equations to the evaluation of stresses developing in a steel vacuum vessel with inner radius $R_1 = 3$m and outer radius $R_2 = 3.5$m as a result of irradiation are illustrated in Fig. 4. The form of function $\omega_{rel}(r)$ used as input reflects the fact that neutron flux from an isotropic source varies as a function of $r$ as $\omega_{rel}(r) \sim r^{-2}$ and also that neutrons are absorbed in the material over a characteristic distance of a fraction of a meter.

Figure 4 shows that particularly high stresses develop close to the internal surface of the steel shell even if the amount of damage accumulated in the material is relatively small. The characteristic magnitude of radiation-induced stresses can be estimated by evaluating the product of the shear modulus of the material and function $\omega_{rel}(\mathbf{r})$, averaged over the volume of the component.

## VII. FINITE ELEMENT IMPLEMENTATION

The finite element implementation of the mathematical formalism for computing strains, stresses and swelling of irradiated reactor components developed above, is based on equation (29), which can be written in the form

$$f_i(\mathbf{r}) = -B\frac{\partial}{\partial x_i}\omega_{rel}(\mathbf{r}), \quad (49)$$

where $B = 2\mu(1+\nu)/[3(1-2\nu)]$ is the bulk modulus of the material and $\omega_{rel}(\mathbf{r})$ is the density of relaxation volumes of defects (21).

The fundamental equation for the stress tensor, defining the condition of mechanical equilibrium, has the form

$$\frac{\partial}{\partial x_j}\sigma_{ij}(\mathbf{r}) + f_i(\mathbf{r}) = 0. \quad (50)$$

To find the displacement field which satisfies (50) using the finite element method, this expression for mechanical equilibrium is recast as a virtual work expression; for completeness this is outlined here. Multiplying (50) by an arbitrary displacement field $\delta u_i$ which satisfies $\delta u_i = 0$ on the displacement boundary $S_u$, and integrating over the body $V$ gives:

$$\int_V \left(\frac{\partial \sigma_{ij}}{\partial x_j} + f_i\right)\delta u_i dR^3 = 0. \quad (51)$$

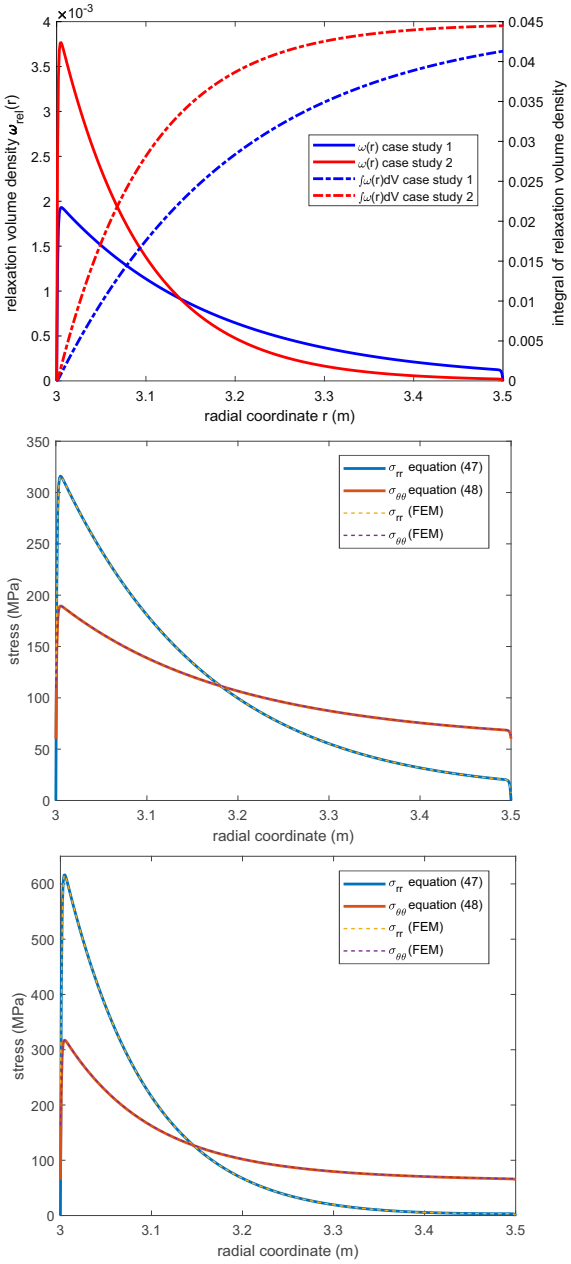


FIG. 4: Top: assumed distributions of relaxation volume densities of defects $\omega_{rel}(r)$ and their integrals $\int_{R1}^{r}\omega_{rel}(R)dV$ in a spherical steel shell with inner radius of $R_1 = 3$m and outer radius of $R_2 = 3.5$m. Middle and bottom graphs show radial and hoop stresses in the component computed using equations (47), (48) and FEM using the relaxation volume densities, given in the top graph, as input. The shear modulus of steel is $\mu = 80$ GPa, $\nu = 0.29$. For comparison, the yield strength of Eurofer97 ferritic-martensitic steel is 530 MPa[60].

Consider the first term

$$\int_V \frac{\partial \sigma_{ij}}{\partial x_j}\delta u_i dR^3 = \int_V \frac{\partial}{\partial x_j}\left(\sigma_{ij}\delta u_i\right) dR^3 - \int_V \sigma_{ij}\frac{\partial}{\partial x_j}\delta u_i dR^3. \tag{52}$$

Using the divergence theorem, the first term on the right hand side is

$$\int_V \frac{\partial}{\partial x_j}\left(\sigma_{ij}\delta u_i\right) dR^3 = \int_S \sigma_{ij}\delta u_i n_j dR^2 = \int_{S_t} \delta u_i \bar{t}_i dR^2 \tag{53}$$

where $\bar{t}_i = \sigma_{ij}n_j$ are the specified surface tractions on $S_t$ and by definition the virtual displacement $\delta u_i = 0$ on $S_u$ and so the surface integral vanishes there. Therefore, after multiplying by $-1$, (51) becomes

$$\int_V \sigma_{ij}\frac{\partial}{\partial x_j}\delta u_i dR^3 - \int_V f_i \delta u_i dR^3 - \int_{S_t} \bar{t}_i \delta u_i dR^2 = 0. \tag{54}$$

Expressing the stress tensor in terms of displacements,

$$\sigma_{ij} = \frac{1}{2}C_{ijkl}\left(\frac{\partial u_k}{\partial x_l} + \frac{\partial u_l}{\partial x_k}\right) = C_{ijkl}\frac{\partial u_k}{\partial x_l} \tag{55}$$

due to the symmetry of $C_{ijkl}$. Therefore

$$\int_V C_{jikl}\frac{\partial u_k}{\partial x_l}\frac{\partial \delta u_i}{\partial x_j}dR^3 - \int_V f_i\delta u_i dR^3 - \int_{S_t}\bar{t}_i\delta u_i dR^2 = 0. \tag{56}$$

This is the expression for virtual work in the presence of a body force $f_i$. This can be discretised and solved at the FE nodes located at $X_i^a$ where $1 < a < m$, for the unknown displacement at each node $U_i^a$. The virtual displacement and it's derivative are interpolated using the shape functions

$$\delta u_i(\mathbf{r}) = \sum_{a=1}^{m} N^a(\mathbf{r})\delta U_i^a \tag{57}$$

$$\frac{\partial \delta u_i(\mathbf{r})}{\partial x_j} = \sum_{a=1}^{m}\frac{\partial N^a(\mathbf{r})}{\partial x_j}\delta U_i^a \tag{58}$$

The displacement derivative is interpolated in a similar manner, namely

$$\frac{\partial u_k(\mathbf{r})}{\partial x_l} = \sum_{b=1}^{m}\frac{\partial N^b(\mathbf{r})}{\partial x_l}U_k^b \tag{59}$$

where $N^a(\mathbf{r})$ is the nodal shape function of node $a$ which satisfies

$$N^a(\mathbf{r}^b) = \delta_{ab}. \tag{60}$$

Substituting (57)-(59) into (56) gives

$$\left[\int_V C_{ijkl}\frac{\partial N^b(\mathbf{r})}{\partial x_l}U_k^b\frac{\partial N^a(\mathbf{r})}{\partial x_j}d^3R - \int_V f_i(\mathbf{r})N^a(\mathbf{r})d^3R - \int_{S_t}\bar{t}_i(\mathbf{r})N^a(\mathbf{r})d^2R\right]\delta U_i^a = 0 \tag{61}$$

and as the virtual displacement $\delta U_i^a$ is arbitrary, the term in square brackets must be zero. In matrix form, the following system of equations is obtained

$$K_{ik}^{ab} U_k^b = F_i^a \quad \text{if } X_k^b \text{ not on } S_u \tag{62}$$

$$U_k^b = \bar{u}_k(\mathbf{r}) \text{ if } X_k^b \text{ on } S_u \tag{63}$$

where

$$K_{ik}^{ab} = \int_V C_{ijkl} \frac{\partial N^a(\mathbf{r})}{\partial x_j} \frac{\partial N^b(\mathbf{r})}{\partial x_l} d^3R \tag{64}$$

$$F_i^a = \int_V f_i(\mathbf{r}) N^a(\mathbf{r}) d^3R + \int_{S_t} \bar{t}_i(\mathbf{r}) N^a(\mathbf{r}) d^2R. \tag{65}$$

$K_{ik}^{ab}$ is the global stiffness matrix. $F_i^a$ is the global force vector which includes a body force contribution at every node not on $S_u$, and surface traction contribution $\bar{t}_i$ for nodes on $S_t$. Substituting the body force $f_i(\mathbf{r})$ from (49) into (65) gives

$$F_i^a = -B \int_V \frac{\partial \omega_{rel}(\mathbf{r})}{\partial x_i} N^a(\mathbf{r}) d^3R + \int_{S_t} \bar{t}_i(\mathbf{r}) N^a(\mathbf{r}) d^2R \tag{66}$$

The advantage of using the body force is that it has a remarkably simple form (49). If $\omega_{rel}(r)$ is an analytic function which can be differentiated then the global force vector $F_i^a$ can be specified exactly, and the nodal displacements obtained by inverting the global stiffness matrix. If only numerical values of $\omega_{rel}^c$ are known at the nodal positions $X_i^c$, then the gradient of the density of defect relaxation volumes required to obtain the body force can instead be evaluated using the finite element shape functions, in the same manner as for the displacements,

$$\frac{\partial}{\partial x_i} \omega_{rel}(\mathbf{r}) = \sum_{c=1}^{n} \frac{\partial N^c(\mathbf{r})}{\partial x_i} \omega_{rel}^c \tag{67}$$

A body force can easily be implemented in a commercial finite element code such as *Abaqus*[61] through the *DLOAD* user subroutine to specify $f_i(\mathbf{r})$ at every integration point. The finite element implementation was first validated by simulating the spherical shell solved analytically in section VI. Due to the symmetry of the problem only one quarter of the shell was simulated with symmetry boundary conditions applied. An elastic isotropic material law was used with $\nu = 0.29$ and $\mu = 80$ GPa. A convergence study was performed, and 1 mm size antisymmetric elements (CAX4) were found to produce excellent agreement with the analytic solution, as shown in Fig. 4. Simulations were also performed for the modified case where

$$\omega_{rel}(\mathbf{r}) = \begin{cases} 0 & \text{if } 0 \le \theta \le \pi/9 \\ \omega_{rel}(r) & \text{if } \pi/9 < \theta \le \pi \end{cases}$$

this represents the case where neutrons are shielded with 20° of the upper pole of the spherical shell. As the body force is no longer symmetric in $\theta$, half of the spherical shell was simulated, and $\sigma_{\theta\theta}$ differs from $\sigma_{\phi\phi}$. The shear stress $\theta_{r\theta}$ is also non-zero near the interface between the shielded and unshielded region.

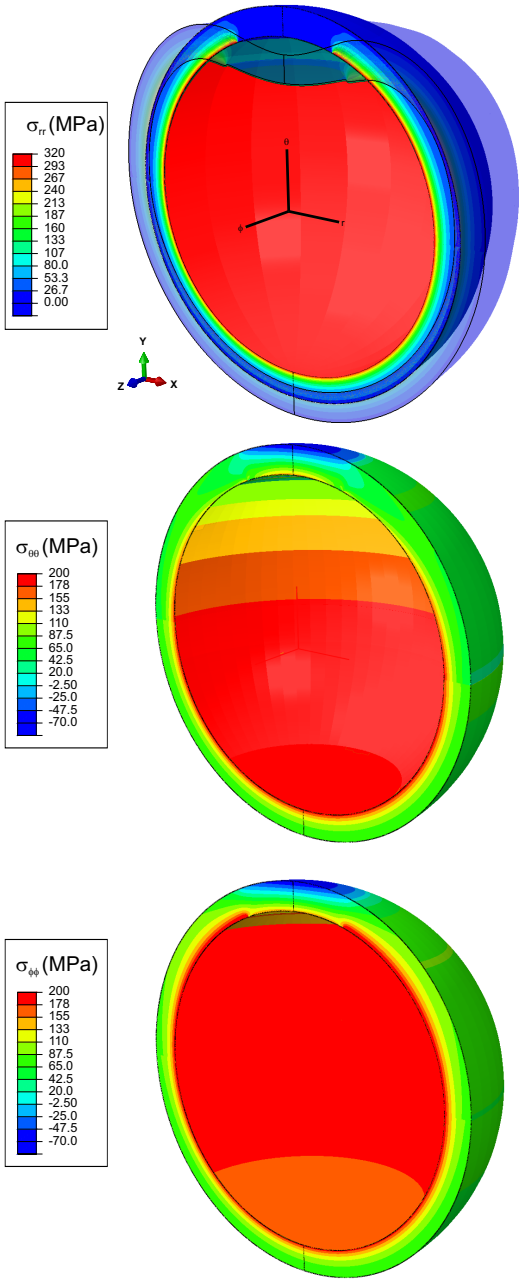


FIG. 5: The radial stress $\sigma_{rr}$ calculated using FEM with the top of the sphere shielded, $\omega(r,\theta) = 0$ for $\theta < 20°$. The deformed mesh is superimposed with the deformation scaled by 200. Parameters as in case study 1. The $\sigma_{\theta\theta}$ and $\sigma_{\phi\phi}$ components are shown in the middle and lower figure with the same colour scale.

## VIII. CONCLUSIONS

The treatment developed in this paper shows how to compute strains, stresses and swelling of fusion reactor components resulting from the accumulation of defects in materials exposed to irradiation. By deriving the fundamental macroscopic equations from atomic scale, we find

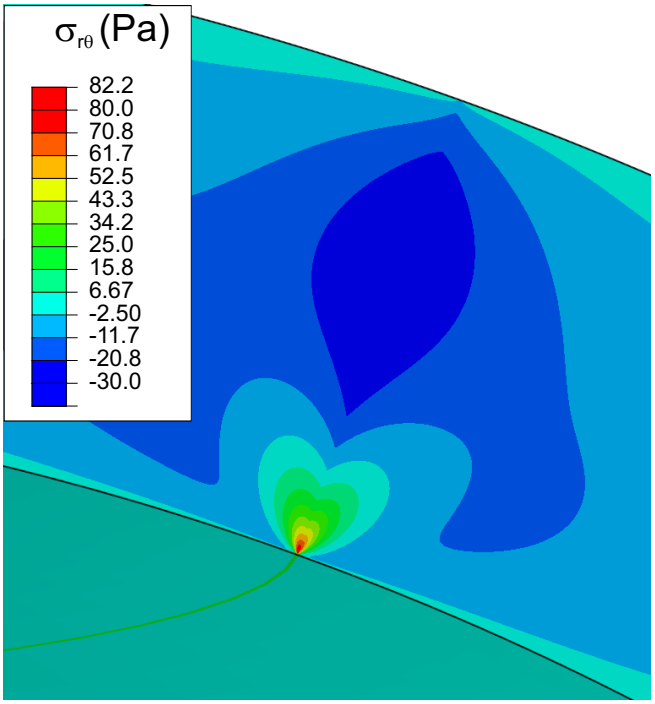


FIG. 6: The shear stress $\sigma_{r\theta}$ calculated using FEM with the top of the sphere shielded, $\omega(r,\theta) = 0$ for $\theta < 20^{\circ}$. The deformed mesh is superimposed with the deformation scaled by 200. Parameters as in case study 1. The $\sigma_{\theta\theta}$ and $\sigma_{\phi\phi}$ components are shown in the middle and lower figure with the same colour scale.

that populations of defects accumulating in the materials under irradiation produce internal body forces (29), (49) that result in the build-up of internal stresses and cause macroscopic deformation of irradiated components. The central notion of the treatment is the spatially varying density of relaxation volumes of defects (21), which acts as a source of stresses and strains, and the gradient of which generates the spatially distributed body force. We illustrate applications of the method using exact analytical solutions and numerical finite element implementations, which suggest that the method is able to provide a reasonably accurate first-principles based foundation for the *in silico* engineering assessment of operational performance of a fusion power plant and its design.

### Acknowledgments

This work has been carried out within the framework of the EUROfusion Consortium and has received funding from the Euratom research and training programme 2014-2018 under grant agreement No 633053 and from the RCUK Energy Programme [grant number EP/P012450/1]. The views and opinions expressed herein do not necessarily reflect those of the European Commission. We would like to acknowledge valuable discussions with A.P. Sutton, C.H. Woo, F. Hofmann, M. Rieth, and J. W. Connor. SLD is grateful to I. Lindsey and M.M.E. Coolsen who enabled this research to be carried out. ET acknowledges support from EPSRC through fellowship grant, EP/N007239/1. AES acknowledges support from the Academy of Finland through project No. 311472.

[1] W. G. Wolfer, *The dislocation bias*, J. Computer-Aided Mater. Des. **14**, 403 (2007)
[2] S. L. Dudarev, Pui-Wai Ma, *Elastic fields, dipole tensors, and interaction between self-interstitial atom defects in bcc transition metals*, Phys. Rev. Materials **2**, 033602 (2018)
[3] F. Hofmann, D. Nguyen-Manh, M.R. Gilbert, C.E. Beck, J.K. Eliason, A.A. Maznev, W. Liu, D.E.J. Armstrong, K.A. Nelson, S.L. Dudarev, *Lattice swelling and modulus change in a helium-implanted tungsten alloy: X-ray micro-diffraction, surface acoustic wave measurements, and multiscale modelling*, Acta Materialia **89**, 352 (2015)
[4] A.D. Brailsford and R. Bullough, *The rate theory of swelling due to void growth in irradiated metals*, J. Nucl. Mater. **44**, 121 (1972)
[5] R. Bullough, B.L. Eyre and K. Krishan, *Cascade damage effects on the swelling of irradiated materials*, Proc. Royal Society London A **346**, 81 (1975)
[6] A.D. Braisford and R. Bullough, *The theory of sink strengths*, Philos. Trans. Roy. Soc. **302**, 81 (1981)
[7] I.G. Margvelashvili and Z.K. Saralidze, *Influence of an elastic field of a dislocation on steady-state diffusion fluxes of point defects*, Sov. Phys. Solid State **15**, 1774 (1974)
[8] P. T. Heald, *The preferential trapping of interstitials at dislocations*, Philos. Mag. **31**, 551 (1975)
[9] P.H. Dederichs and K. Schroeder, *Anisotropic diffusion in stress fields*, Phys. Rev. B**17**, 2524 (1978)
[10] C. H. Woo, *The sink strength of a dislocation loop in the effective medium approximation*, J. Nucl. Mater. **98**, 279 (1981)
[11] N.V. Doan and G. Martin, *Elimination of irradiation point defects in crystalline solids: sink strengths*, Phys. Rev. B**67**, 134107 (2003)
[12] Z. Chang, P. Olsson, D. Terentyev, N. Sandberg, *Multi-scale calculations of dislocation bias in fcc Ni and bcc Fe model lattices*, Nuclear Instruments and Methods B**352**, 81 (2015)
[13] S.L. Dudarev, A.A. Semenov, and C.H. Woo, *Heterogeneous void swelling near grain boundaries in irradiated materials*, Phys. Rev. B**67**, 094103 (2003)
[14] A.E. Sand, S.L. Dudarev and K. Nordlund, *High-energy collision cascades in tungsten: Dislocation loops structure and clustering scaling laws*, EPL (EuroPhysics Letters), **103** (2013) 46003
[15] A.E. Sand, K. Nordlund, S.L. Dudarev, *Radiation damage production in massive cascades initiated by fusion neutrons in tungsten*, Journal of Nuclear Materials **455** (2014) 207–211
[16] X. Yi, A.E. Sand, D.R. Mason, M.A. Kirk, S.G. Roberts,

K. Nordlund, and S.L. Dudarev, *Direct observation of size scaling and elastic interaction between nano-scale defects in collision cascades*, EPL (EuroPhysics Letters), **110** (2015) 36001

[17] A.E. Sand, M.J. Aliaga, M.J. Caturla, and K. Nordlund, *Surface effects and statistical laws of defects in primary radiation damage: Tungsten vs. iron*, EPL (EuroPhysics Letters), **115** (2016) 36001

[18] A.E. Sand, D.R. Mason, A. De Backer, X. Yi, S.L. Dudarev, and K. Nordlund, *Cascade fragmentation: deviation from power law in primary radiation damage*, Mater. Res. Lett., **5** (2017) 357–363

[19] D.R. Mason, A.E. Sand, X. Yi, S.L. Dudarev, *Direct observation of the spatial distribution of primary cascade damage in tungsten*, Acta Materialia **144**,905 (2018)

[20] G. Leibfried, N. Breuer, *Point Defects in Metals* (Springer, Berlin, 1978), pp. 147-149

[21] A. M. Kossevich, *The Crystal Lattice*, (Wiley-VCH, Berlin, 1999) p. 216

[22] E. Clouet, C. Vervenne, T. Jourdan, *Elastic modelling of point defects and their interactions*, Comput. Mater. Sci. **147**, 49 (2018)

[23] T. Mura, *Micromechanics of Defects in Solids*, (Kluwer, Dordrecht, The Netherlands, 1991) p. 22

[24] C. Varvenne, F. Bruneval, M.-C. Marinica, and E. Clouet, *Point defect modeling in materials: Coupling ab initio and elasticity approaches*, Phys. Rev B**88**, 134102 (2013)

[25] E. Clouet, S. Garruchet, H. Nguyen, M. Perez, C.S. Becquart, *Dislocation interaction with C in α-Fe: A comparison between atomic simulations and elasticity theory*, Acta Materialia **56**, 3450 (2008)

[26] S.L. Dudarev, A.P. Sutton, *Elastic interactions between nano-scale defects in irradiated materials*, Acta Materialia **125**, 425 (2017)

[27] J. P. Hirth and J. Lothe, *Theory of dislocations*, 2nd edition (Krieger, Malabar, Florida, 1992), p. 835

[28] P. H. Dederichs, *The theory of diffuse X-ray scattering and its application to the study of point defects and their clusters*, J. Phys. F: Metal Phys. **3**, 471 (1973)

[29] K. Nordlund, P. Partyka, R.S. Averback, I.K. Robinson, P. Ehrhart, *Atomistic simulation of diffuse X-ray scattering from defects in solids*, J. Appl. Phys. **88**, 2278 (2000)

[30] J. F. Nye, *Physical Properties of Crystals*, (Clarendon Press, Oxford, UK, 1985), p. 132

[31] K. Nordlund, S.J. Zinkle, A, E. Sand, F. Granberg, R.S. Averback, R. Stoller, T. Suzudo, L. Malerba, F. Banhart, W.J. Weber, F. Willaime, S.L. Dudarev, D Simeone, *Improving atomic displacement and replacement calculations with physically realistic damage models*, Nature Communications **9**, 1084 (2018)

[32] L.D. Landau and E.M. Lifshits, *Theory of Elasticity*, 3rd Edition. (Butterworth-Heinemann, Oxford, 1986)

[33] F. Hofmann, E. Tarleton, R. J. Harder, N. W. Phillips, P.-W. Ma, J. N. Clark, I. K. Robinson, B. Abbey, W. Liu and C. E. Beck, *3D lattice distortions and defect structures in ion-implanted nano-crystals*, Scientific Reports **7**, 45993 (2017)

[34] C. C. Fu, F.Willaime, P. Ordejón, *Stability and Mobility of Mono- and Di-Interstitials in α-Fe*, Phys. Rev. Lett. **92**, 175503 (2004)

[35] C.C. Fu, J. Dalla Torre, F. Willaime, J.-L. Bocquet, A. Barbu, *Multiscale modelling of defect kinetics in irradiated iron*, Nature Materials **4**, 68 (2005)

[36] D. Nguyen-Manh, A. P. Horsfield, S. L. Dudarev, *Self-interstitial atom defects in bcc transition metals: Group-specific trends*, Phys. Rev. B**73**, 020101 (2006)

[37] S. L. Dudarev, *Density Functional Theory Models for Radiation Damage*, Annu. Rev. Mater. Res. **43**, 35 (2013).

[38] P.M. Derlet, D. Nguyen-Manh, and S.L. Dudarev, *Multi-scale modelling of crowdion and vacancy defects in body-centered-cubic transition metals*, Phys. Rev. B **76**, 054107 (2007).

[39] G. Kresse and J. Hafner, *Ab initio molecular dynamics for liquid metals*, Phys. Rev. B, **47** 558, 1993.

[40] G. Kresse and J. Hafner, *Ab initio molecular-dynamics simulation of the liquid-metalamorphous-semiconductor transition in germanium*, Phys. Rev. B, **49** 14251, 1994.

[41] G. Kresse and J. Furthmüller, *Efficiency of ab-initio total energy calculations for metals and semiconductors using a plane-wave basis set*, Comput. Mat. Sci., **6** 15, 1996.

[42] G. Kresse and J. Furthmüller, *Efficient iterative schemes for ab initio total-energy calculations using a plane-wave basis set*, Phys. Rev. B, **54** 11169, 1996.

[43] J. P. Perdew, K. Burke, and M. Ernzerhof, *Generalized Gradient Approximation Made Simple*, Phys. Rev. Lett., **77** 3865, 1996.

[44] J. P. Perdew, K. Burke, and M. Ernzerhof, *Erratum on Generalized Gradient Approximation Made Simple [Phys. Rev. Lett.* **77***, 3865 (1996)]*, Phys. Rev. Lett., **78** 1396, 1997.

[45] R. Armiento and A. E. Mattsson, *Functional designed to include surface effects in self-consistent density functional theory*, Phys. Rev. B **72**, 085108 (2005).

[46] A. E. Mattsson and R. Armiento, *Implementing and testing the AM05 spin density functional*, Phys. Rev. B **79**, 155101 (2009).

[47] A. E. Mattsson, R. Armiento R, J. Paier, G. Kresse, J. M. Wills, and T. R. Mattsson, *The AM05 density functional applied to solids*, J. Chem. Phys **128**, 084714 (2008).

[48] M.-C. Marinica, L. Ventelon, M. R. Gilbert, L. Proville, S. L. Dudarev, J. Marian, G. Bencteux, and F. Willaime, *Interatomic potentials for modelling radiation defects and dislocations in tungsten*, J. Phys: Condens. Mater. **125**, 395502 (2013)

[49] J. A. Zimmerman, E.B. Webb, J.J. Hoyt, R.E. Jones, P.A. Klein, and D.J. Bammann, *Calculation of stress in atomistic simulation*, Modelling Simul. Mater. Sci. Eng. **12**, S319 (2004).

[50] C. Björkas, K. Nordlund, and S. L. Dudarev. *Modelling radiation effects using the ab-initio based tungsten and vanadium potentials.*, Nucl. Instr. Meth. B, **267** 3204–3208 (2009).

[51] A.E. Sand and K. Nordlund, *On the lower energy limit of electronic stopping in simulated collision cascades in Ni, Pd and Pt*, J. Nucl. Mater. **456** 99–105 (2015)

[52] H.J.C. Berendsen, J.P.M. Postma, W.F. van Gunsteren, A. DiNola, and J.R. Haak *Molecular dynamics with coupling to an external bath*, J. Chem. Phys., **81** 3684–3690, (1984).

[53] A. E. Sand, D. R. Mason, A. De Backer, X. Yi, S. L. Dudarev and K. Nordlund, *Cascade fragmentation: deviation from power law in primary radiation damage*, Mater. Res. Lett. **5**, 357–363 (2017)

[54] A. Stukowski, *Visualization and analysis of atomistic simulation data with OVITO - the Open Visualization Tool*, Modelling Simul. Mater. Sci. Eng. **18**, 015012 (2010).

[55] M.R. Gilbert, S.L. Dudarev, S. Zheng, L.W. Packer and J.-Ch. Sublet, *An integrated model for materials in a fusion power plant: transmutation, gas production, and helium*

*embrittlement under neutron irradiation*, Nucl. Fusion **52** (2012) 083019

[56] M.R. Gilbert, S.L. Dudarev, D. Nguyen-Manh, S. Zheng, L.W. Packer, J.-Ch. Sublet, *Neutron-induced dpa, transmutations, gas production, and helium embrittlement of fusion materials*, Journal of Nuclear Materials **442** (2013) S755-S760

[57] M.R. Gilbert, J. Marian, J.-Ch. Sublet, *Energy spectra of primary knock-on atoms under neutron irradiation*, Journal of Nuclear Materials **467** (2015) 121-134

[58] I. Rovelli, S.L. Dudarev, A.P. Sutton, *Non-local model for diffusion-mediated dislocation climb and cavity growth*, Journal of the Mechanics and Physics of Solids **103** (2017) 121-141

[59] T.D. Swinburne, K. Arakawa, H. Mori, H. Yasuda, M. Isshiki, K. Mimura, M. Uchikoshi, S. L. Dudarev, *Fast, vacancy-free climb of prismatic dislocation loops in bcc metals*, Scientific Reports **6** (2016) 30596

[60] P. Fernández, A.M. Lancha, J. Lapeña, M. Serrano, M. Hernández-Mayoral, *Metallurgical properties of reduced activation martensitic steel Eurofer97 in the as-received condition and after thermal ageing*, Journal of Nuclear Materials **307-311** (2002) 495-499

[61] *Abaqus 2016 Documentation*, (Dassault Systèmes, Providence, RI, USA. 2016)